Journal of Applied Fluid Mechanics, Vol. 16, No. 7, pp. 1427-1441, 2023.
Available online at www.jafmonline.net, ISSN 1735-3572, EISSN 1735-3645.
https://doi.org/10.47176/jafm.16.07.1655

Optimization Design of a Semi-Open Centrifugal Impeller using GA-Fuzzy Logic Combination Strategy

F. Zhang[1], Y. Heng[2, 3], Q. Liu[1], R. Tao[1, 3, 4†], W. Yang[1,4], D. Zhu[5] and R. Xiao[1, 4]

[1] *College of Water Resources and Civil Engineering, China Agricultural University, Beijing, 100083, China*
[2] *School of Energy and Power engineering, Xihua University, Chengdu, Sichuan Province, 610039, China*
[3] *Key Laboratory of Fluid and Power Machinery, Ministry of Education, Xihua University, No. 9999 Hongguang Avenue, Pidu District, Chengdu 610039, China*
[4] *Beijing Engineering Research Center of Safety and Energy Saving Technology for Water Supply Network System, China Agricultural University, Beijing, 100083, China*
[5] *College of Engineering, China Agricultural University, Beijing, 100083, China*

†*Corresponding Author Email: randytao@cau.edu.cn*

(Received November 12, 2022; accepted March 6, 2023)

Abstract

Semi-open centrifugal pump has the disadvantage of low efficiency in chemical industry for its unique structure. For the purpose of improving its efficiency as much as possible on the premise of meeting the head demand, in this case, an optimization strategy combining Bezier curve, Genetic Algorithm (GA), Fuzzy Logic (FL), Artificial Neural Network (ANN) and solution space model based on stratified sampling is proposed to optimize the efficiency of semi-open centrifugal pump. The fourth-order Bezier curve is used as parametric method to control the blade profile, GA combined with FL is used as optimization strategy to seek the optimal individual. Besides, the optimization solution space based on stratified sampling method and ANN training are used to shorten computing time. Finally, the semi-open centrifugal pump corresponding to the optimal parameter combination of blade profile has been found, and on the premise of meeting the head requirements, the efficiency has been significantly improved. Entropy production rate is carried out to analyze the reason of efficiency improvement. The whole optimization strategy proposed in this study provides a good reference for parametric control and performance optimization of bladed pump.

Key words: Centrifugal pump; Semi-open impeller; Genetic Algorithm; Fuzzy Logic; Optimization design.

NOMENCLATURE

b	width of the overflow section	v_2	absolute speed at blade outlet
c	constant of correction term	v_m	axial component of absolute velocity
D	diameter of impeller	v_u	circumferential component of absolute velocity
D_e	orthogonal divergence term		
e	dissipation rate	w	relative velocity
E_{pro}	entropy production rate	w_1	relative speed of the blade inlet
f	turbulent eddy frequency	w_2	relative speed of the blade outlet
G_k	kinetic energy of turbulence	Z	blades number
g	gravitational acceleration	α_1	absolute flow angle at the blade inlet
H	head of centrifugal pump	α_2	absolute flow angle at the blade outlet
H_d	design pump head	β	model closure constant
k	turbulent kinetic energy	β_1	placement angle of the blade inlet
L	blade height	β_2	placement angle of the blade outlet
M	impeller torque	δ	value of the clearance between hub and blade
n_d	design speed of impeller	ε	energy loss nearby the solid wall
Δp	static pressure difference at the pump inlet and pump outlet	ε_{ini}	energy loss nearby the solid wall of each component for initial pump
Q	flow rate	ε_{opt}	energy loss nearby the solid wall of each component for optimized pump
Q_d	design flow rate		
R_1	inner radius of the backward swept blade	η	efficiency
R_2	outer radius of the backward swept blade	θ	wrap angle of blade

r	radius of the circumference where the fluid particle is located
s	percentage of blade spanwise distribution
T	temperature
t	blade thickness
u_1	circumferential speed of the blade inlet
u_2	circumferential speed of the blade outlet
V	volume nearby the wall less than 2 mm
v_1	absolute speed at blade inlet
$\Delta\theta'$	average value of the difference between each point on Bezier curves and on spline curve
$\Delta\theta_i$	the θ value difference between each point on Bezier curves and on spline curve
$\Delta\theta_{SD}$	Bezier curves of each order
ρ	fluid density
ω	impeller angular velocity

1. INTRODUCTION

Semi-open centrifugal pump has great anti-blocking performance, it is convenient and clean for its unique structural form (Li 2011; Jia *et al.* 2022). Semi-open centrifugal pump is commonly used in aerospace, petrochemical industry, chemical industry, medical pharmaceutical industry, municipal construction and many other fields (Gölcü *et al.* 2010). For chemical industry, the semi-open structure improves the anti-blocking performance when delivering chemical reagent, but it also leads to low efficiency (Ayad *et al.* 2016). However, for turbomachine, blade wrap angle has an important impact on its energy performance (Choi *et al.* 2006). For semi-open centrifugal pump, the head (H) and efficiency (η) are the main parameters to measure its energy performance (Tao *et al.* 2019; Hu *et al.* 2022; Wei *et al.* 2021). Therefore, it is significant to improve the efficiency of semi-pen centrifugal pump by optimizing the blade wrap angle.

In common one-dimensional design method of turbomachine, the blade wrap angle is usually defined as the included angle between the meridian plane of a fluid particle on the blade streamline and the initial meridian plane (Bai *et al.* 2017). Then, the basic shape of blade profile is obtained by giving the blade profile differential equation controlled by blade wrap angle. In addition, according to the stiffness and strength requirements of the pump impeller and different applications, thicken the impeller with different thickness variation laws (Wang *et al.* 2021). Basing on the one-dimensional design method of turbomachinery, Ju *et al.* (2018) researched the influence of blade shape changing on hydraulic performance of vortex pump, and introduced 2D and 3D corner blades for the design of vortex pump. Siddique *et al.* (2022) and Namazizadeh *et al.* (2019) found that the blade shape of impeller will affect the maximum efficiency of centrifugal pump and did some optimization researches on how splitter blades influence the pump performance. Wu *et al.* (2019) have applied the method of improving the pump efficiency by optimizing blade profile to a sewage self-priming pump. According to the above studies, continuity of the blade profile differential equation controlled by blade wrap angle in one-dimensional design method often brings trouble to the optimization process of the pump. For the continuously changing curve, in order to reduce the control parameters of the curve, the method of "replacing curve with straight" is often adopted. However, it changes the variety law of some points and is not accurate enough for controlling the impeller blade wrap angle.

In 1962, French engineer Pierre Bezier developed a method to determine the control points according to the known curve parameter equation, so as to draw a smooth curve (Feng *et al.* 2018). Many scholars have also done relevant research on the in-depth exploration and extended application of Bezier curve. Moreau *et al.* (2019 a, b) and Hu *et al.* (2019) researched path planning for autonomous vehicle basing on Bezier curve, and they have gotten great effect. Li *et al.* (2014) combined Bezier curve and firefly algorithm for path planning, which obtained superior success rate. Tharwat *et al.* (2019) used optimization algorithm of chaotic particle swarm combined with Bezier curves to find optimal path. In this research, the Bezier curve with fourth-order is used to control the change of impeller blade wrap angle. After the order convergence analysis, it not only ensures the accuracy of the control curve, but also reduces the control parameters, which brings great convenience for the subsequent optimization of impeller blade wrap angle to improve pump efficiency.

Optimization design based on intelligent algorithm has always been a hot topic in turbomachine. As an early developed evolutionary algorithm, Genetic Algorithm has also been widely used to design the centrifugal pump. Homaifar *et al.* (1994) optimized turbofan system and found the optimal combination of key parameters of turbofan by Genetic Algorithm. Lampinen (Lampinen 2003) researched preliminary design and shape optimization of cam profiles for cam operated mechanisms basing on GA. Zhu *et al.* (2019) have optimized leading-edge of a mixed-flow pump impeller with GA. Boukhobza *et al.* (2022) designed the orthogonal filter banks to compress speech by GA. Previous studies have shown that GA has certain advantages in the process of optimization.

In summary, there are still some gaps to be filled in the existing research. On the one hand, there is little research on the parametric control of blade wrap angle to optimize the energy performance of centrifugal pump. On the other hand, the existing research has not solved the problem of slow convergence and easy to fall into local optimization of GA, and has not formed a systematic optimization strategy. The gaps above are not conducive to the improvement of the optimization method system for centrifugal pump research.

In this research, for a semi-open centrifugal pump, the fourth-order Bezier curve will be used to control the geometry of the blade profile, the optimization strategy combines GA, FL, ANN and the solution

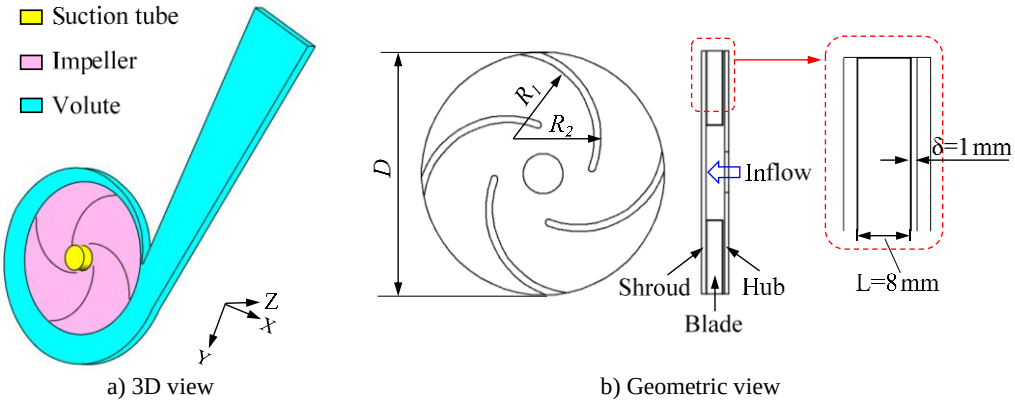

a) 3D view b) Geometric view

Fig. 1. Model of objective pump and impeller.

Table 1 Main parameters of impeller.

Parameters	Value	Unit
Blades number Z	4	[-]
Diameter of impeller D	120	mm
Blade height L	8	mm
Blade thickness t	3.5	mm
Inner radius R_1	41.5	mm
Outer radius R_2	45	mm

space of parameter combination based on stratified sampling is proposed to improve efficiency of objective pump. After optimization, to know the optimization mechanism, entropy analysis of optimization results will be carried out.

2. RESEARCH MODEL AND RESEARCH THEORY

2.1 Pump Geometry and Test Rig

As shown in Fig. 1, the research objective of this study is a semi-open centrifugal pump with open experiment data (Choi *et al.* 2004). The suction tube, impeller and volute constitute the main flow domains. The geometric parameters of the impeller are shown in Table 1, among them, the blade type is traditional backward swept blade, and R_1 and R_2 represent the inner and outer radius of the blade respectively. There is a uniform equivalent clearance between hub and blade whose value (δ) is 1mm. The rated speed n_d of impeller is 700r/min, and the design flow rate Q_d is 0.4745kg/s, besides, the design head H_d is 0.8m. In this study, the optimization work will be carried out according to the working conditions corresponding to the design flow rate, with design head as the constraint and the efficiency as the optimization goal.

In addition to the geometric parameters, the specific speed n_s reflects the geometric parameters and performance of pump. It is expressed as follows:

$$n_s = \frac{3.65n\sqrt{Q}}{H^{3/4}} \tag{1}$$

In this research, the calculated n_s is about 60.28.

Figure 2 is the schematic diagram of test rig, in which the pressure difference at pump inlet and outlet is measured by differential pressure gauge; the torque of the impeller is measured by the torque gauge.

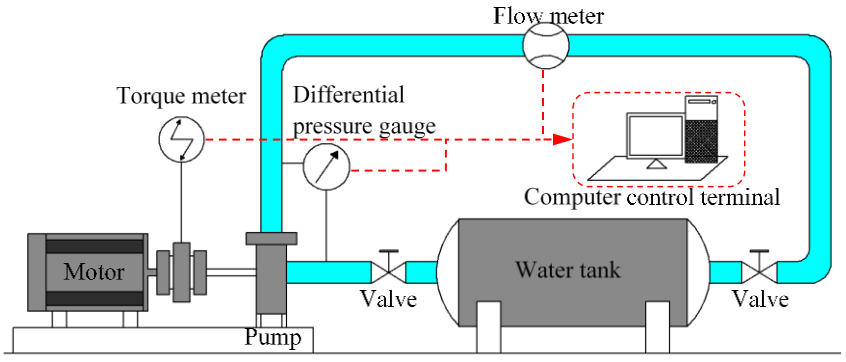

Fig. 2. Map of test rig.

In the whole research process, whether it is experimental or numerical simulation, the head H of centrifugal pump is calculated by Eq. (2); and efficiency η is defined by Eq. (3):

$$H = \frac{\Delta p}{\rho g} \tag{2}$$

Where, ρ represents fluid density, g represents gravitational acceleration, Δp represents static pressure difference at the pump inlet and pump outlet.

$$\eta = \frac{\Delta p \cdot Q}{2\pi n M} \tag{3}$$

Where M represents impeller torque.

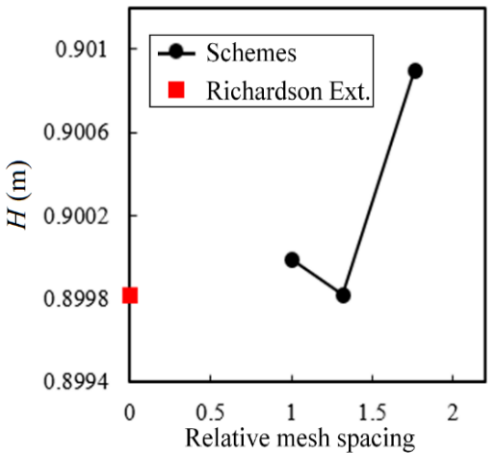

Fig. 3. Index values of GCI meshing check schemes.

2.2 CFD Setup

The numerical simulation part is based on the commercial software ANSYS CFX turbulence solver and the theory of Computational Fluid Dynamics (CFD). In the process of numerical simulation, it is of great importance to select a suitable turbulence model. SST k-ω turbulence model has the characteristics of good convergence and high stability. It can enhance the solution of wall function and avoid the situation that the grid near the wall is too dense, and it makes the solution result not so sensitive to the wall grid (Menter *et al.* 2003). Therefore, this study finally selected SST k-ω model as turbulence prediction model. Governing equations of turbulent kinetic energy and turbulent dissipation rate are as follows:

$$\frac{\partial}{\partial t}(\rho k) + \frac{\partial}{\partial x_i}(\rho k u_i) = \frac{\partial}{\partial x_j}\left(\Gamma_k \frac{\partial k}{\partial x_j}\right) + G_k - Y_k + S_K \tag{4}$$

$$\frac{\partial}{\partial t}(\rho e) + \frac{\partial}{\partial x_i}(\rho e u_i) = \frac{\partial}{\partial x_j}\left(\Gamma_e \frac{\partial e}{\partial x_j}\right) + G_e - Y_e + D_e + S_e \tag{5}$$

Where, k represents turbulent kinetic energy, e represents dissipation rate, Γ_k represents the diffusion term of k, Γ_e represents diffusion term of e, G_k represents kinetic energy of turbulence, D_e represents the orthogonal divergence term, Y_k represents divergence term of k, Y_e represents divergence term of e.

For the numerical simulation settings, the inlet of the whole fluid domain is the inlet of suction tube, and the outlet of the whole fluid domain is the outlet of the volute. Among them, the inlet of fluid domain is set as the pressure boundary and the outlet of fluid domain is set as the mass flow rate boundary. In order to use wall function, the y+ value on all the wall boundary is adjusted between 30 and 100 which effectively guarantees the convergence of the solution process of wall function. In addition, the General Grid Interface (GGI) mesh connection method is set to ensure the reliability of interface data transmission. In the whole pump, only the impeller is a rotating component and the rest components are stationary. All the walls in flow domain are set as non-slip wall. The maximum number of iteration steps is set as 500, and the convergence criterion of momentum equation and continuity equation is 10^{-5}.

For the fluid domain meshing, the suction tube and impeller are meshed with hexahedral structured mesh, and the volute is meshed with tetrahedral unstructured mesh. In order to make sure the results of numerical simulation are reliable, the grid independence analysis is carried out based on Richardson extrapolation (GCI) (Celik *et al.* 2008). The details are shown in Fig. 3. The total number of coarse, medium and fine (N1, N2 and N3) mesh schemes are 560186, 1288413 and 3031168 respectively. The refinement factor of the first mesh scheme N1 compared with the second mesh scheme N2 is represented by r_{21} and its value is 1.32. Similarly, the refinement factor of the second mesh scheme N2 compared with the third mesh scheme N3 is represented by r_{32} and its value is 1.33. Under the design flow rate, the pump head H is set as the key parameter to evaluate the convergence of grid independence check. Through the calculation, the GCI value of fine mesh scheme is 0.013%, and that of coarse mesh scheme is 0.0012%, both of them are less than 5%, meeting the convergence requirements. Comprehensively considering the grid convergence index and computing resources, the second mesh scheme is selected as the final mesh scheme for this study. Table 2 shows the grids number of each component, and the mesh scheme of the whole fluid domain is shown in Fig. 4.

Table 2 Grids number of each component.

Components	Element type	Node number
Suction tube	Hexahedral structured mesh	59850
Impeller	Hexahedral structured mesh	1127191
Volute	Tetrahedral unstructured mesh	101372
Total	Mixed	1288413

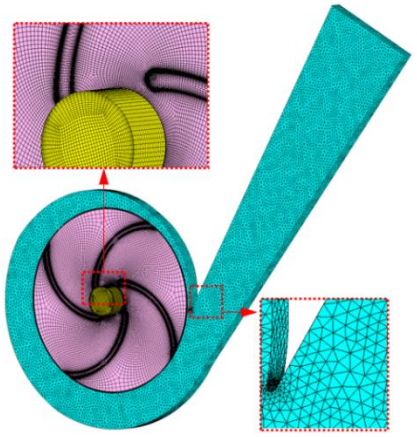

Fig. 4. Mesh scheme of whole fluid domain.

2.3 Energy Performance

Based on the energy performance experimental data of the objective pump tested by Choi *et al*. (2004), the flow rate corresponding to the highest efficiency is the design flow rate which is 1.0Q_d. The values of 0.1Q_d to 1.3Q_d are taken as the flow rate value to numerical simulation. The head and efficiency corresponding to each mass flow rate are calculated, then the energy performance curves of are obtained by numerical simulation. In Fig. 5, comparing the experimental results with the numerical simulation results, it shows that with the flow rate increasing,

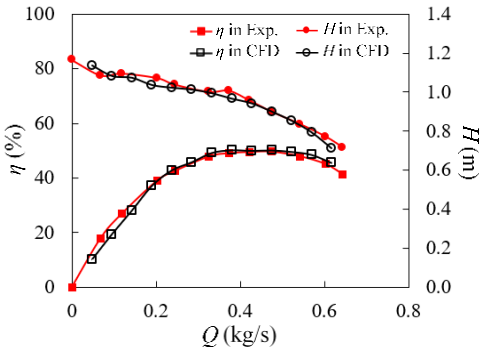

Fig. 5. Comparative curves of energy performance.

the trend of pump efficiency and pump head of two modes are in good agreement. The error between the numerical simulation results and experimental results is within 5%, which shows that the numerical simulation results are fully credible based on the previous numerical settings.

2.4 Parameterization

Figure 6a) is the 3D schematic diagram of the objective semi-open centrifugal pump impeller, in which L represents a spatial streamline on the impeller blade. In order to express the shape of the spatial streamline, Fig. 6b) is the plane projection of the impeller and streamline while Fig. 6c) is axial plane projection of the impeller and streamline. ω represents the rotation direction of the impeller, u_1 and u_2 represent the circumferential speed of the blade inlet and outlet respectively; v_1 and v_2 respectively represent the absolute speed at blade inlet and outlet; w_1 and w_2 represent the relative speed of the blade inlet and outlet respectively. Besides, β_1 and β_2 respectively represents the placement angle of the blade inlet and outlet, α_1 and α_2 respectively represents the absolute flow angle at the blade inlet and outlet, θ represents the blade wrap angle.

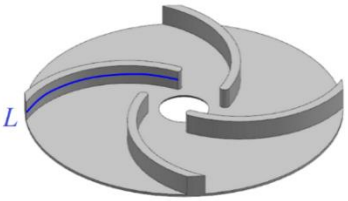

a) 3D schematic diagram of objective pump impeller

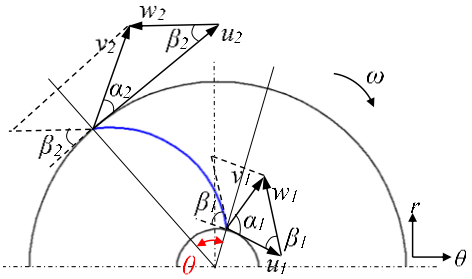

b) Plane view

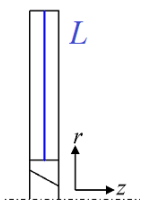

c) Axial view

Fig. 6. Geometric expression of spatial streamline.

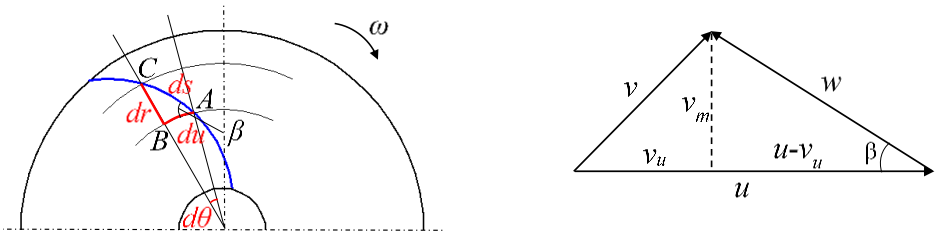

a) Streamline element b) Velocity triangle

Fig. 7. Micro element expression of spatial streamline.

As shown in Fig. 7a), take a micro element of blade spanwise *ds* on the streamline, and its corresponding blade wrap angle is *dθ*, besides, the micro element in the circumferential direction is *du* and the micro element in the radial direction is *dr*. According to the relationship between the sides and angles of the geometric triangle, the following relationship can be obtained in the triangle ABC:

$$\tan\beta = \frac{BC}{AB} = \frac{ds}{du} \tag{6}$$

Where:

$$du = r \cdot d\theta \tag{7}$$

The velocity triangle of any fluid particle on the blade profile is shown in Fig. 7b), where v_m represents the axial component of absolute velocity and v_u represents the circumferential component of absolute velocity. According to the relationship among the sides and angles of the velocity triangle, Eq. (8) can be obtained:

$$\tan\beta = \frac{v_m}{u - v_u} \tag{8}$$

Combining Eq. (6) and Eq. (8), Eq. (9) can be obtained:

$$ds = \frac{v_m}{u - v_u} r d\theta \tag{9}$$

Where, $u=\omega r$. Eq. (10) can be reached by substituting Eq. (9):

$$d\theta = \frac{\omega r^2 - v_u r}{v_m r^2} ds \tag{10}$$

Combining the relationship between the sides and angles of triangle ABC and velocity triangle in Fig. 7b), Eq. (11) can be expressed as following:

$$\frac{dr}{ds} = \sin\beta = \frac{v_m}{w} \tag{11}$$

For the axial component of absolute velocity, it can be expressed by Eq. (12):

$$v_m = \frac{Q}{2\pi r b} \tag{12}$$

Where, *r* represents the radius of the circumference where the fluid particle is located, and *b* represents the width of the overflow section.

Combined Eq. (11) and Eq. (12), Eq. (13) can be obtained:

$$r dr = \frac{Q}{2\pi b w} ds \tag{13}$$

Equation (14) can be obtained by integrating both sides of Eq. (13) at the same time:

$$r^2 = \frac{Q}{\pi b w} s \tag{14}$$

Substitute Eq. (14) into Eq. (10) to obtain:

$$d\theta = \left(\frac{\omega}{v_m} - \frac{v_u}{v_m \sqrt{\frac{Q}{\pi b w}}} \cdot \frac{1}{\sqrt{s}} \right) ds \tag{15}$$

Integrate both sides at the same time to obtain Eq. (16):

$$\theta = \frac{\omega}{v_m} s - \frac{2 v_u}{v_m \sqrt{\frac{Q}{\pi b w}}} \cdot \sqrt{s} + c \tag{16}$$

Thus, the functional relationship between the blade wrap angle of blade profile and the percentage of spanwise distribution is obtained, where *c* represents the constant of correction term, ω represents impeller angular velocity, v_m represents axial component of absolute velocity, v_u represents circumferential component of absolute velocity, *w* represents relative velocity, *Q* represents flow rate, *s* represents the percentage of blade spanwise distribution, 0<s<1.

If the continuous function relationship is used to accurately express the impeller blade profile, there are too many control points being required. However, in 1962, Bezier curve was proposed and widely published by French engineer Pierre Bezier. The characteristic of this curve is that a smooth curve can be obtained through a small number of control points. Usually, at least four points are used to control the curve, which are starting point, the ending point and

two middle sliding points. Bezier curve with the number of n+1 control point is defined as n-order Bezier curve. For a given P_0, P_1, P_2...P_n, n-order general Bezier curve formula can be expressed by Eq. (17):

$$\begin{aligned} B(t) &= \sum_{i=0}^{n} {}_i^n P_i (1-t)^{n-i} t^i \\ &= \binom{n}{0} P_0 (1-t)^n t^0 + \binom{n}{1} P_1 (1-t)^n t^1 \\ &+ \ldots + \binom{n}{n-1} P_{n-1} (1-t)^1 t^{n-1} \end{aligned} \tag{17}$$

In 2D s-θ coordinate system, the percentage of blade spanwise distribution s and blade wrap angle θ can be expressed as the functions of t, the expression form of third-order Bezier curve is:

$$\begin{cases} s = s_1(1-t)^3 + 3s_2 t(1-t)^2 \\ +3s_3 t^2(1-t) + s_4 t^3 \\ \theta = \theta_1(1-t)^3 + 3\theta_2 t(1-t)^2 \\ +3\theta_3 t^2(1-t) + \theta_4 t^3 \end{cases} \tag{18}$$

The fourth-order Bezier curve can be expressed as:

$$\begin{cases} s = s_1(1-t)^4 + 4s_2 t(1-t)^3 \\ +6s_3 t^2(1-t)^2 + 4s_4 t^3(1-t) + s_5 t^4 \\ \theta = \theta_1(1-t)^4 + 4\theta_2 t(1-t)^3 \\ +6\theta_3 t^2(1-t)^2 + 4\theta_4 t^3(1-t) + \theta_5 t^4 \end{cases} \tag{19}$$

The fifth-order Bezier curve can be expressed as:

$$\begin{cases} s = s_1(1-t)^5 + 5s_2 t(1-t)^4 \\ +10s_3 t^2(1-t)^3 + 10s_4 t^3(1-t)^2 \\ +5s_5 t^4(1-t) + s_6 t^5 \\ \theta = \theta_1(1-t)^5 + 5\theta_2 t(1-t)^4 \\ +10\theta_3 t^2(1-t)^3 + 10\theta_4 t^3(1-t)^2 \\ +5\theta_5 t^4(1-t) + \theta_6 t^5 \end{cases} \tag{20}$$

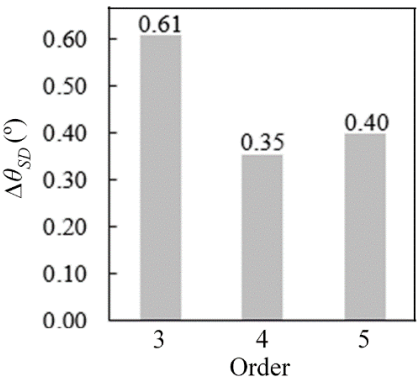

Fig. 8. Convergence analysis of each order Bezier curves

Similarly, the expression of higher-order Bezier curves can be obtained. Substituting the expressions of third-order, fourth-order and fifth-order Bezier curves into Eq. (16), the coordinate expression of Bezier curves can be obtained.

In this study, the convergence of third-order, fourth-order and fifth-order Bezier curves are analyzed. Take the ten s_i points (i =1, 2, …, 9, 10) with equidistant value which corresponding to the spline s-θ curve and Bezier s-θ curve of each order respectively, the standard deviation between spline curve and Bezier curves of each order $\Delta\theta_{SD}$ are given by Eq. (21):

$$\Delta\theta_{SD} = \sqrt{\frac{1}{10}\sum_{i=1}^{10}\left(\Delta\theta_i - \Delta\theta'\right)^2} \tag{21}$$

Where, $\Delta\theta_i$ represents the θ value difference between each point on Bezier curves and on spline curve; $\Delta\theta'$ represents the average value of the difference between each point on Bezier curves and on spline curve.

The convergence analysis results of each order Bezier curve are shown in Fig. 8, which shows that the curve under the control of the fourth-order Bezier curve is the closest to the spline curve. Therefore, the fourth-order Bezier curve with five control points is selected as control curve in this study.

Figure 9 is the schematic diagram of the fourth-order Bezier control curve finally selected in this study, that is, the percentage of blade spanwise distribution and the blade wrap angle curve (s-θ curve) are controlled by the fourth-order Bezier curve with five control points. The coordinates of each point are (s_1, θ_s), (s_2, θ_1), (s_3, θ_2), (s_4, θ_3), (s_5, θ_e). Since the impeller blade wrap angle is the difference of inlet and outlet blade wrap angle, in order to further reduce the optimization parameters, the θ_s value of starting point is fixed, and the spanwise percentage distribution of the five control points is fixed, that is, s_1=0, s_2=15, s_3=30, s_4=60, s_5=100. In the end, the final variables only are the blade wrap angles of three sliding points θ_1, θ_2, θ_3 and of ending points θ_e. In order to make sure the structural rationality of blade, within reasonable bending and torsion range of blade, the value ranges of each optimization parameter are given in Table 3.

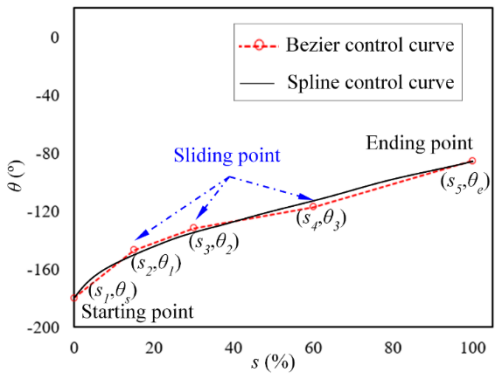

Fig. 9. Schematic diagram of fourth-order Bezier curve.

Table 3 Value range of each control parameter.

Parameters	θ_1	θ_2	θ_3	θ_e
Ranges	(-80°, -150°)	(-70°, -140°)	(-60°, -130°)	(-50°, -120°)

In this study, the efficiency of objective pump is set as the optimization goal, the head higher than design head value (0.8m) is set as the constraint. The detail optimization is carried out with the four control parameters.

3. OPTIMIZATION THEORY

Figure 10 is the flow chart of the whole optimization process in this study. After realizing the parametric control of the blade, the solution space of the whole optimization is constructed by means of stratified sampling, and the optimization is carried out by using the GA combined with FL. After accumulating certain CFD numerical simulation results, in order to improve the optimization speed, ANN is trained and used in the whole solution space for further optimization. The whole optimization process is judged as convergence when the efficiency of the optimal individual keeps unchanged for eight generations. The optimal efficiency and its corresponding parameter combination are obtained.

3.1 Solution Space Construction Based on Stratified Sampling

Before the algorithm optimization, in order to ensure that the sample structure is similar to the overall structure, so as to improve the accuracy of the whole ANN, stratified sampling is used to construct the solution space of the whole optimization. As shown in Fig. 11, the value range of each parameter is

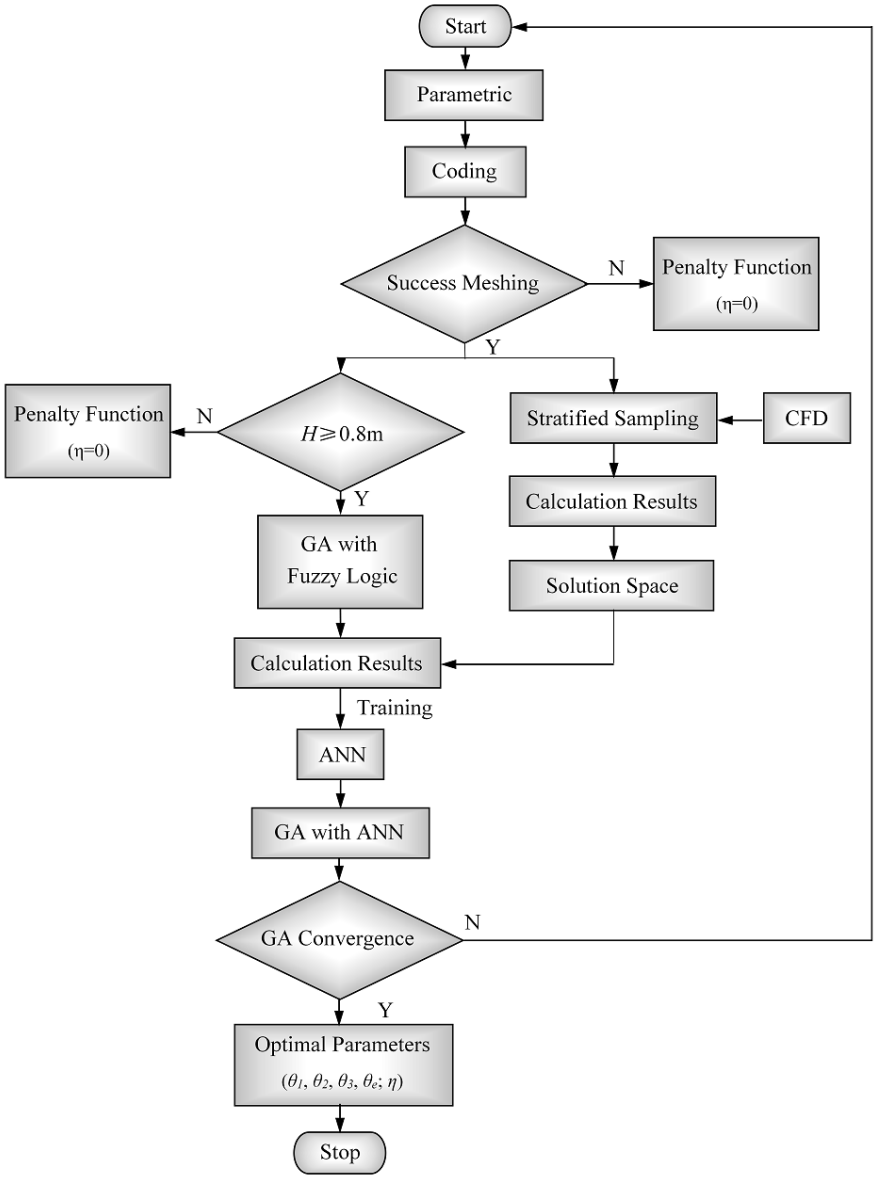

Fig. 10. Diagram of the optimization process.

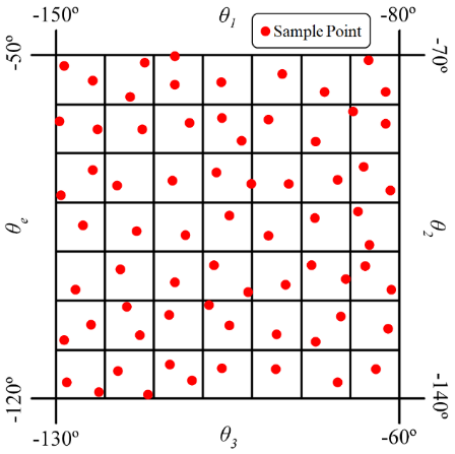

Fig. 11. Ann solution space based on stratified sampling.

equally divided into seven intervals, and a θ value is randomly selected in each interval, combining four points θ values randomly. From 7^4 random parameter combinations, 70 samples are evenly selected for efficiency calculation with CFD numerical simulation, and the solution space of the whole optimization is constructed.

3.2 Fuzzy Logic

Fuzzy Logic is defined as the process and way of judgment and reasoning that imitate the concept of uncertainty in the human brain. For the model position or uncertain description system, fuzzy set and fuzzy rules are used for reasoning, so as to solve the problem. As shown in Fig. 12, based on the fuzzy controller, the probability of crossover, mutation, duplication and elimination of GA is fuzzily controlled in this study.

3.3 Genetic Algorithm (GA)

Basing on Genetic Algorithm, this study optimizes the blade profile parameters combinations corresponding to the optimal efficiency of objective pump. GA is an optimization algorithm to meet the final goal by gradually obtaining better individuals through a series of genetic operations, such as crossover, mutation, duplication and elimination (Bagchi and Pal 2011).

By way of expressing the parameters of optimization and promoting optimization process, binary coding is used to encode the four control parameters. The combination of the coding string of the four parameters represents an individual, and the number of coding string bits represents its accuracy. In this study, 8-bit binary coding string is used to express a parameter, that is, an individual containing four

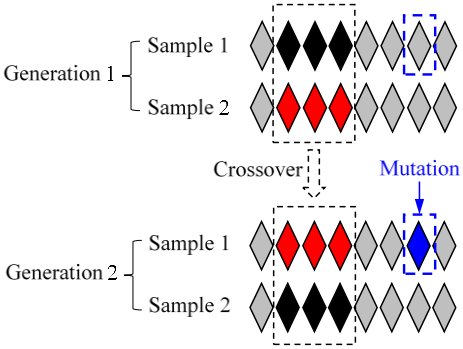

Fig. 13. Schematic diagram of genetic operations.

parameters is expressed by 32-bit binary coding string. Here, ten individuals are taken as a generation, and the first generation of individuals are ten sample individuals generated randomly.

In each generation, the operations of crossover, mutation, duplication and elimination are carried out. Crossover refers to the exchange of coding strings between two individuals, which means that the genetic information carried on the coding string is also exchanged between individuals to form two new individuals. The number of interchangeable coding strings represents the crossover probability. Mutation refers to the change for one or several codes of an individual coding string, so as to change the genetic information carried on the coding string and form a new individual. The purpose of mutation is to jump out of the local optimum trap and find the global optimal result. The number of change codes represents the probability of mutation. Duplication and elimination refer to comparison in one generation which contains ten individuals, replacing the individuals which least meet the optimization objectives with the individuals which most meet the optimization objectives, and preserving the good genetic genes to the next generation. Fig. 13 is schematic diagram of these genetic operations.

probability and elimination and duplication probability of GA are expressed in combination with FL. In addition, for the untenable examples that cannot generate grid or do not meet the head requirement, the penalty function is used to multiply its efficiency by the penalty factor 0 to eliminate it. The IF-THEN expressions are as follows:

3.4 GA with FL and ANN

Even though Genetic Algorithm is applied in many optimization examples, it also faces the disadvantages that the convergence rate is slow and easily falls into the local optimum trap. Therefore, in order to speed up the convergence rate of GA and avoid falling into local optimum in the optimization

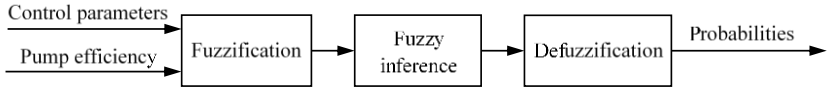

Fig. 12. Schematic diagram of fuzzy solver.

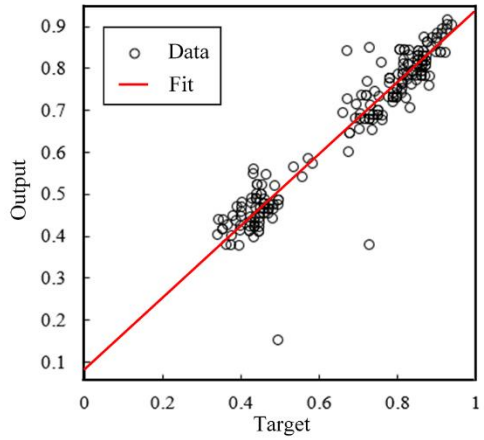

Fig. 14. ANN training regression.

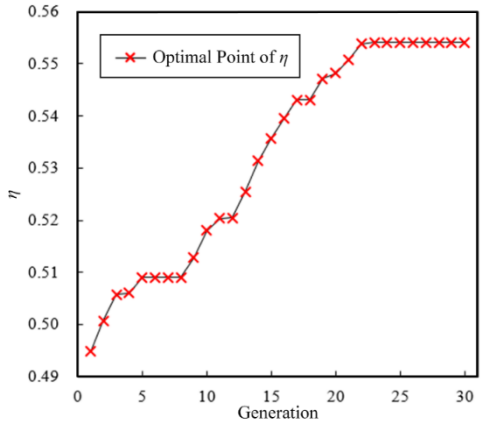

Fig. 15. Optimization result.

process, the crossover probability, mutation

IF failed to generate grid, IS error case, THEN efficiency multiplied by penalty factor 0.

IF succeed to generate grid, IS good case, THEN calculate the efficiency and check whether the head constraint is met.

IF H<0.8m, IS error case, THEN efficiency multiplied by penalty factor 0.

IF H>0.8m, IS good case, THEN enter the GA with FL system.

All individuals in each generation of GA are sorted, and their mutation probability, crossover probability, duplication and elimination probability are given according to their own system ranking. In this study, IF-THEN of GA with FL system is expressed as follows:

IF ranking 1 or 2, IS high efficiency cases, THEN mutation probability is 3.125%, crossover probability is 0%, duplication and elimination probability is 100%.

IF ranking 3 to 7, IS medium efficiency cases, THEN mutation probability is 10%, crossover probability is 12.5%, duplication and elimination probability is 0%.

IF ranking 8 to 10, IS low efficiency cases, THEN mutation probability is 8.3%, crossover probability is 6.25%, duplication and elimination probability is 100%.

The GA with FL can adjust the probability of crossover, mutation, duplication and elimination according to the optimization process of GA itself, so as to improve the convergence rate and jump out of local optimum trap. The optimization algorithm in this study is based on an ANN solution space under stratified sampling, combined with the GA based on FL to obtain 100 CFD calculation results after 10 generations, and ANN is trained to complete the whole optimization process. In this study, 70% samples are used for training, 15% for testing and 15% for validation. As shown in Fig. 14, the value of ANN regression R obtained by training is about 0.976. The corresponding efficiency of the optimal individuals of each generation in the whole optimization process is shown in Fig. 15.

4. Analysis Of Optimization Result

4.1 Geometric and Energy Performance Comparison

Basing on the GA with FL and the ANN combined with stratified sampling, the GA results remain unchanged for 8 consecutive generations after 30 generations of optimization. At this time, it is considered that the GA has reached convergence in this study. As shown in Fig. 16, the initial blade wrap angle is 95º, and the optimized blade wrap angle is 112º, that is, the shape of blade is optimized from the original straight blade with equal thickness to the twisted blade with equal thickness.

As shown in Table 4 and Fig. 17, for the optimized pump, the efficiency is increased by 5.220% compared with the initial pump, but the pump head

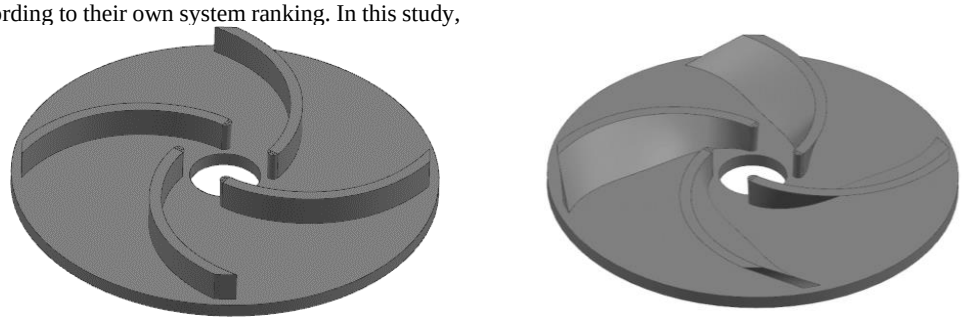

(a) Initial (b) Optimized

Fig. 16. Comparison of blade shape before and after optimization.

Table 4 Comparison of energy performance.

	Experiment	Initial CFD	Optimized CFD
Pump head H (m)	0.898	0.898	0.855
Pump Efficiency η (%)	49.699	50.194	55.414

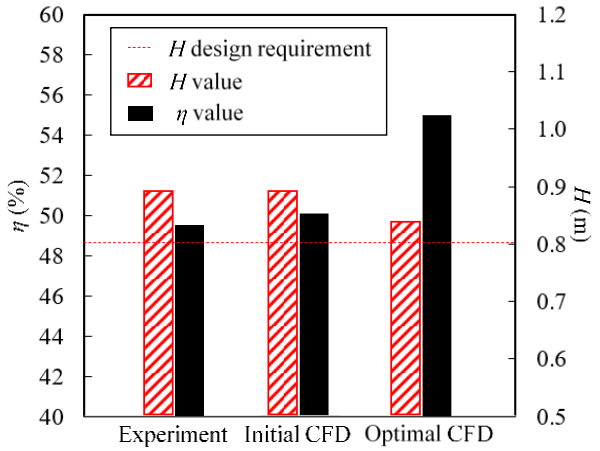

Fig. 17. Comparison of energy performance between experiment and CFD.

is only reduced by 0.043m, which still meets the design requirements that the objective pump head is greater than 0.8m. In other words, through the optimization method in this study, on the premise of meeting the head requirements, the efficiency of studied semi-open centrifugal pump in this research is effectively improved, and practical problems in engineering application of chemical industry are solved.

4.2 Entropy Production Rate Comparison

Entropy production rate E_{pro} is usually defined to express the flow energy loss inside pump (Kock and Herwig 2004; Zhou *et al.* 2018). In order to analyze the mechanism of optimization results, the entropy analysis is carried out. The value of E_{pro} is positively correlated with the amount of energy loss. Its definition is:

$$E_{pro} = \frac{\beta \rho f k}{T} \tag{22}$$

where β represents the model closure constant, it is given as β = 0.09 here, f represents turbulent eddy frequency, k represents turbulent kinetic energy, ρ represents fluid density, and T represents temperature, here T = 20 °C.

Figure 18 shows the contour of E_{pro} and streamline of velocity for different sections of the impeller. Among them, Fig. 18a) shows the contour at shroud span. It can be seen that there is a certain energy loss at leading edge of the initial blade, but for the optimized impeller, the overall energy loss nearby the shroud surface is small. Fig. 18b) shows the E_{pro} contour and velocity streamline for the middle span of the blade are shown. It shows that for the initial impeller, the energy loss is large at edge of the vortex, and the optimized blade shape is distorted, the flow pattern in the blade channel has improved as well. This is because for the initial impeller, there is a trend of outward diffusion, which intensifies the energy loss. However, the optimized curved and twisted blade suppresses the diffusion trend of the vortex and tightens the vortex inward, which leaded low energy loss. Fig. 18c) shows the E_{pro} contour and velocity streamline for the middle span of the clearance of the semi-open impeller. It indicated that for the initial impeller, the energy loss in impeller clearance is large due to the influence of the blade wall surface. However, in optimized impeller whose blades are curved and twisted, the blade wall influence on the flow in the clearance is weakened, and the energy loss in the clearance is significantly reduced.

Figure 19 shows E_{pro} contour of the axial middle span of the suction tube and impeller before and after optimization. It indicated that for initial contour, the energy loss of impeller clearance, the solid wall at leading edge and the trailing edge of the blade are very serious, and the energy loss has been significantly improved in the optimized pump.

As shown in Fig. 20, on the 0.5 streamwise, the E_{pro} contour of the middle span is shown, there is an obvious area with high energy loss in the blade channel of initial impeller, which has a large area, presents a whole large high energy loss group, and this area has a certain diffusion trend. However, for the optimized impeller, the region with high energy loss disappears, and the region with sub-high energy loss presents small energy loss group, which are not connected into pieces and have no diffusion trend.

For giving further analysis of the change of energy loss nearby the solid wall between initial impeller and optimized impeller, the entropy production rate is volume integrated to research the energy loss

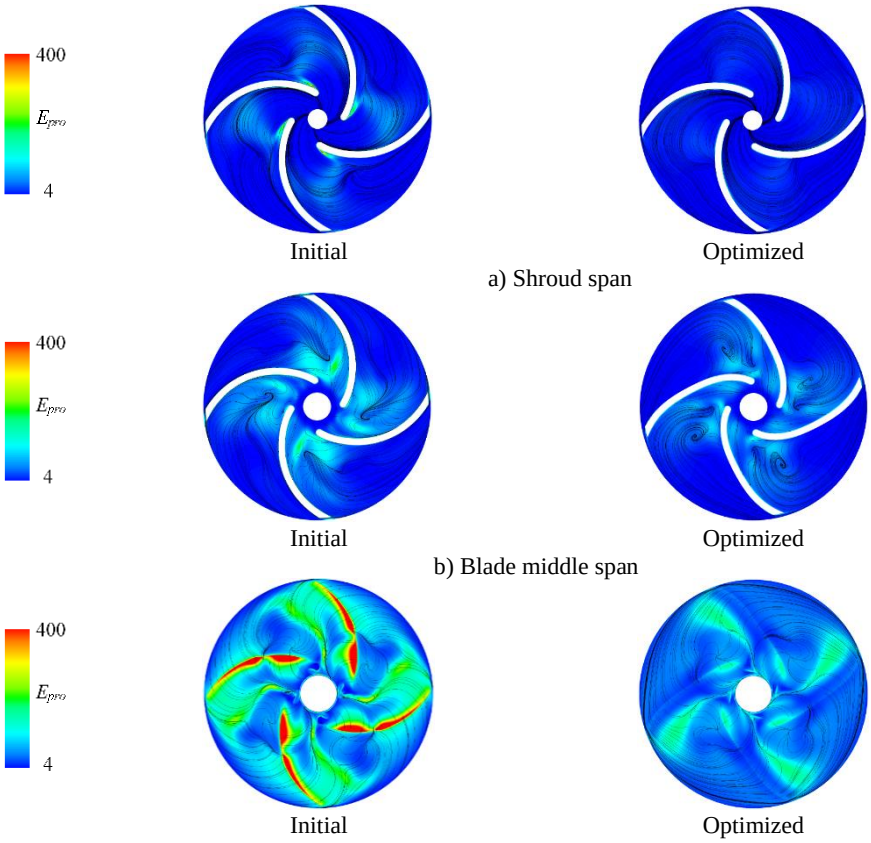

Fig. 18. Comparison of E_{pro} contour and velocity streamline for different spans.

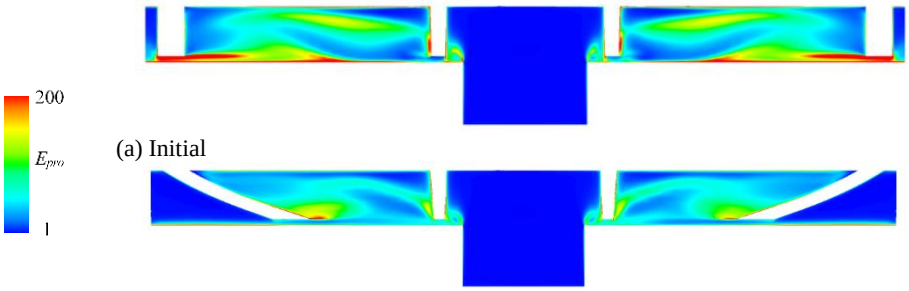

Fig. 19. Comparison of E_{pro} contour for axial middle span.

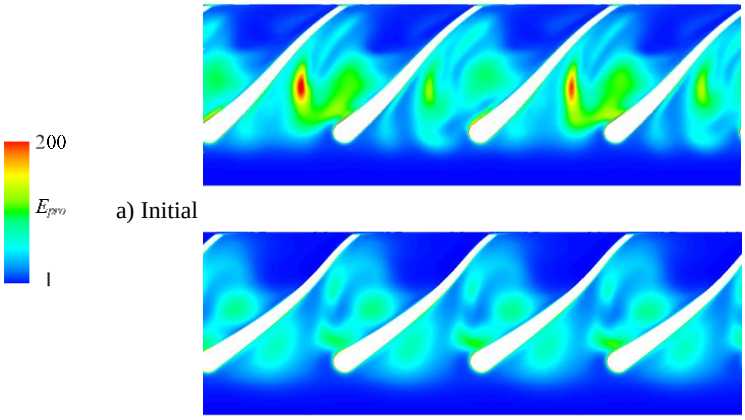

Fig. 20. Comparison of E_{pro} contour for 0.5 streamwise.

Table 5 Comparison of energy loss nearby the solid wall for each component.

Component	ε_{ini} (10^{-3}W·m^{-3}K^{-1})	ε_{opt} (10^{-3}W·m^{-3}K^{-1})
Suction Tube	0.005	0.005
Impeller	3.404	2.068
Volute	0.095	0.075

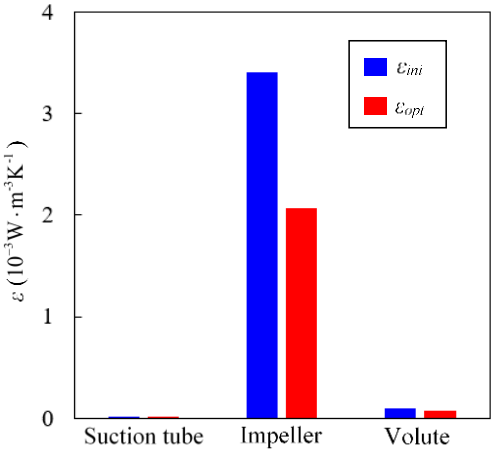

Fig. 21. Comparison of energy loss nearby the solid wall for different components.

nearby the solid wall of each component of the objective pump, in which the energy loss nearby the solid wall is defined as ε. The specific calculation formula is as follows:

$$\varepsilon = \int E dV \tag{23}$$

Where, V represents the volume nearby the wall less than 2 mm which is the defined nearby-wall region.

Table 5 shows the data of energy loss nearby the solid wall before and after optimization of each component, and Fig. 21 visually shows the comparison of energy loss nearby the solid wall before and after optimization. where ε_{ini} represents the energy loss nearby the solid wall of each component for initial pump, ε_{opt} represents the energy loss nearby the solid wall of each component for optimized pump. It can be seen that the energy loss nearby the solid wall in the pump is mainly concentrated on the impeller component. For the optimized pump, the energy loss nearby the solid wall of the impeller decreases by 39.25%, while the energy loss nearby the solid wall in the suction tube and volute is very small and almost negligible.

5. CONCLUSIONS

For improving the efficiency of a semi-open centrifugal pump, the fourth-order Bezier curve is used as the parameterization method, and the Genetic Algorithm, Fuzzy Logic and Artificial Neural Network are combined as the optimization strategy to optimize the change rule of blade wrap angle. In addition, the optimization results are analyzed by analyzing the energy loss inside the pump and near the solid wall. The following conclusions are drawn:

(1) Basing on the fourth-order Bezier curve, the parameter control of the blade profile of the semi-open centrifugal pump impeller is carried out, and then combining with the GA based on FL, the scheme is feasible for the optimization of the overall efficiency of the objective pump.

(2) For the objective semi-open centrifugal pump impeller studied, the efficiency can be improved through optimizing the variation law of the blade wrap angle. Through the analysis of the optimization process, appropriately increasing the blade wrap angle at impeller inlet and outlet can effectively reduce energy loss in the pump and improve pump efficiency.

(3) The energy loss in semi-open impeller is mainly related to the energy loss nearby the solid wall of the impeller and the energy loss in the impeller clearance affected by the solid wall of the blade. Through the optimization of the blade profile, the energy loss can be reduced to a certain extent.

ACKNOWLEDGEMENTS

The author would like to thank the strong supported by the Open Research Subject of Key Laboratory of Fluid and Power Machinery (Xihua University), Ministry of Education, grant number LTDL-2022009; and the National Natural Science Foundation of China, grant number 52079142.

DECLARATIONS

All authors declare that there is no conflict of interest in the publication of this paper.

REFERENCE

Ayad, A. F., H. M. Abdalla and A. A. E. Aly (2016). Effect of semi-open impeller side clearance on the centrifugal pump performance using CFD. *Aerospace Science and Technology* 47,247-255.

Bagchi, P. and S. Pal (2011). *Controlling Crossover Probability in Case of a Genetic Algorithm.* Springer Berlin Heidelberg.

Bai, Y., F. Kong, S. Yang, K. Chen and T. Dai (2017). Effect of blade wrap angle in hydraulic turbine with forward-curved blades. *International Journal of Hydrogen Energy* 42(29), 18709-18717.

Boukhobza, A., N. Taleb, A. Taleb-Ahmed and A. Bounoua (2022). Design of orthogonal filter banks using a multi-objective genetic algorithm for a speech coding scheme. *Alexandria Engineering Journal* 61(10), 7649-7657.

Celik, I. B., U. Ghia, P. J. Roacheand and C. J. Freitas (2008). Procedure for estimation and reporting of uncertainty due to discretization in CFD applications. *Journal of Fluids Engineering-Transactions of the ASME* 130(7).

Choi, Y. D., K. Nishino, J. Kurokawa and J. Matsui (2004). PIV measurement of internal flow characteristics of very low specific speed semi-open impeller. *Experiments in Fluids* 37(5), 617-630.

Choi, Y., J. Kurokawa and J. Matsui (2006). Performance and internal flow characteristics of a very low specific speed centrifugal pump. *Journal of Fluids Engineering-Transactions of the ASME* 128(2), 341-349.

Feng, L., P. Alliez, L. Busé, H. Delingette and M. Desbrun (2018). Curved optimal delaunay triangulation. *ACM Transactions on Graphics* 37(4), 1-16.

Gölcü, M., Y. Pancar, H. Ergür and E. Göral (2010). Prediction of head, efficiency, and power characteristics in a semi-open impeller. *Mathematical and Computational Applications* 15(1), 137-147.

Homaifar, A., H. Lai and E. Mccormick (1994). System optimization of turbofan engines using genetic algorithms. *Applied Mathematical Modelling* 18(2), 72-83.

Hu, Y., D. Li, Y. He and J. Han (2019). Path planning of ugv based on bezier curves. *Robotica* 37(6), 969-997.

Hu, Z., F. Yang, X. Wang, Y. Wu, H. Gao, D. Zhu and R. Tao (2022). Feasibility analysis of detached eddy simulation in tip leakage flow simulation. *Large Electric Machine and Hydraulic Turbine* 5, 59-67.

Jia, X., Q. Chu, L. Zhang and Z. Zhu (2022). Experimental study on operational stability of centrifugal pumps of varying impeller types based on external characteristic, pressure pulsation and vibration characteristic tests. *Frontiers in Energy Research* 10.

Ju, Y., S. Liu and C. Zhang (2018). Effect of blade shape on hydraulic performance and vortex structure of vortex pumps. *Journal of Hydrodynamics Series B* 30(3), 499-506.

Kock, F. and H. Herwig (2004). Local entropy production in turbulent shear flows: a high-Reynolds number model with wall functions. *International Journal of Heat and Mass Transfer* 47(10-11), 2205-2215.

Lampinen, J. (2003). Cam shape optimisation by genetic algorithm. *Computer-Aided Design* 35(8), 727-737.

Li, B., L. Liu, Q. Zhang, D. Lv, Y. Zhang, J. Zhang and X. Shi (2014). Path planning based on firefly algorithm and Bezier curve. *IEEE International Conference on Information and Automation (ICIA)*, Hailar, Peoples R China.

Li, H. (2011). Flow in a dirty air fan with a semi-open centrifugal impeller and a squirrel volute. *Proceedings of the Institution of Mechanical Engineers, Part C: Journal of Mechanical Engineering Science* 225(4), 869-883.

Menter, F. R., M. Kuntz and R. Langtry (2003). Ten years of industrial experience with the sst turbulence model. *Turbulence Heat and Mass Transfer* 4(1), 625-632.

Moreau, J., P. Melchior, S. Victor, L. Cassany, M. Moze, F. Aioun and F. Guillemard (2019a). Reactive path planning in intersection for autonomous vehicle. *IFAC-PapersOnLine* 52(5), 109-114.

Moreau, J., P. Melchior, S. Victor, M. Moze, F. Aioun and F. Guillemard (2019b). Reactive path planning for autonomous vehicle using bezier curve optimization. In *30th IEEE Intelligent Vehicles Symposium (IV)*, Paris, France.

Namazizadeh, M., M. T. Gevari, M. Mojaddam and M. Vajdi (2019). Optimization of the splitter blade configuration and geometry of a centrifugal pump impeller using design of experiment. *Journal of Applied Fluid Mechanics* 13(1), 89-101.

Siddique, M. H., A. Samad and S. Hossain (2022). Centrifugal pump performance enhancement: Effect of splitter blade and optimization. *Proceedings of the Institution of Mechanical Engineers, Part A: Journal of Power and Energy* 236(2), 391-402.

Tao, R., R. Xiao, F. Wang and W. Liu (2019). Improving the cavitation inception performance of a reversible pump-turbine in pump mode by blade profile redesign: Design concept, method and applications. *Renewable Energy* 133, 325-342.

Tharwat, A., M. Elhoseny, A. E. Hassanien, T., Gabel and A. Kumar (2019). Intelligent bezier

curve-based path planning model using chaotic particle swarm optimization algorithm. *Cluster Computing-The Journal of Networks Software Tools and Applications* 22(2), S4745-S4766.

Wang, L., J. Lu, W. Liao, P. Guo, J. Feng, X. Luo and W. Wang (2021). Numerical investigation of the effect of T-shaped blade on the energy performance improvement of a semi-open centrifugal pump. *Journal of Hydrodynamics* 33(4), 736-746.

Wei, Z., R. Tao, R. Xiao and H. Hu (2021). Hydrodynamic improvement by adding inlet baffles on centrifugal pump for reducing cavitation instabilities. *Journal of Vibration and Control* 1802378870.

Wu, D., Z. Zhu, Y. Ren, Y. Gu and P. Zhou (2019). Influence of blade profile on energy loss of sewage self-priming pump. *Journal of the Brazilian Society of Mechanical Sciences and Engineering* 41(10).

Zhou, Q., L. Xia and C. Zhang (2018). Internal mechanism and improvement criteria for the runaway oscillation stability of a pump-turbine. *Applied Sciences* 8(11), 2193.

Zhu, D., R. Tao and R. Xiao (2019). Anti-Cavitation design of the symmetric leading-edge shape of mixed-flow pump impeller blades. *Symmetry-Basel* 11(1), 1-5.